Paclitaxel-loaded PEGylated Cationic Lipid Nanodiscs and Small Liposomes with Protruding Brush Conformation PEG-chains Show Tumor Penetration and Proapoptotic Caspase-3 Activation

Lorena Simón-Gracia[1], Pablo Scodeller[1,2], William S. Fisher[3], Valeria Sidorenko[1], Victoria M. Steffes[3], Kai K. Ewert[3], Cyrus R. Safinya[3]*, and Tambet Teesalu[1,3]*

[1] Laboratory of Precision and Nanomedicine, Institute of Biomedicine and Translational Medicine, Centre of Excellence for Translational Medicine, University of Tartu, Ravila 14b, 50411 Tartu, Estonia

[2] Centro Nacional de Biotecnología (CNB-CSIC), Calle Darwin 3, 28049 Madrid, Spain

[3] Materials Department, Molecular, Cellular, and Developmental Biology Department, Physics Department, and Biomolecular Science and Engineering Program, University of California, Santa Barbara, California 93106, USA

*Corresponding authors contact information: cyrussafinya@ucsb.edu, tambet.teesalu@ut.ee

Abstract

Novel approaches are required to address the urgent need to develop lipid-based carriers of paclitaxel (PTX) and other hydrophobic drugs for cancer chemotherapy. Carriers based on cationic liposomes (CLs) (e.g. EndoTAG-1®) have shown promise in animal models and advanced to late-stage clinical trials. We recently found that the addition of cone-shaped poly(ethylene glycol)-lipid (PEG-lipid) to PTX-loaded CLs (CLs_{PTX}) drives a transition to a phase of sterically stabilized, higher curvature (smaller) lipid nanoparticles consisting of coexisting PEGylated CLs_{PTX} and PTX-containing nanodiscs (bicelles) ($nanodiscs_{PTX}$). At PEG coverages in the brush regime, these PEGylated CLs_{PTX} and $nanodiscs_{PTX}$ showed significantly improved delivery and cytotoxicity to human cancer cells *in vitro*. Here, we investigated the

PTX loading and stability of the CLs_{PTX} and $nanodiscs_{PTX}$ at high concentration and assessed their circulation half-life and biodistribution *in vivo*. At higher content of PEG-lipid (5 and 10 mol% of a PEG-lipid with PEG molecular weight 5000 g/mol), the mixture of PEGylated CLs_{PTX} and $nanodiscs_{PTX}$ formed almost exclusively particles of sub-micron size and incorporated up to 2.5 mol% PTX without crystallization for at least 20 h. Remarkably, compared to lipid vector preparations containing 2 and 5 mol% PEG5K-lipid (with the PEG chains in the mushroom regime), those at 10 mol% with PEG chains in the extended brush conformation showed significantly more tumor penetration and increased proapoptotic caspase-3 activation in 4T1 breast cancer lesions modeled in immunocompetent mice.

Keywords

Chemotherapy; Paclitaxel; Cationic Liposome; PEGylation; Disc bicelle, Tumor penetration; Triple-negative breast cancer

Introduction

Chemotherapy continues to be a common and effective treatment option for cancer. However, a number of the drugs used in chemotherapy have poor water solubility and therefore must be formulated with a vector (carriers) to enable their use. A prime example of this is the potent cytotoxic drug paclitaxel (PTX)[1-4]. PTX is highly hydrophobic with very low water solubility, and it is ineffective in its insoluble crystalline form. Nonetheless, PTX is one of the most commonly used anti-cancer drugs, with multi-billion dollar sales of PTX-based medicines each year[5-11]. Currently, the most prominent formulations of PTX are Taxol® (where PTX is solubilized using nonionic Kolliphor EL surfactant) and Abraxane® (where PTX is formulated in albumin nanoparticles)[5,12-14]. Serious side effects, both due to the vector and the indiscriminate delivery of PTX throughout the body, are common and dose-limiting for these PTX formulations[15-17]. Major efforts are therefore underway to develop improved PTX vectors for cancer chemotherapy with reduced side effects: novel carrier materials to avoid the hypersensitivity reactions associated with the use of Kolliphor EL (formerly Cremophor EL, polyoxyethylated castor oil), carriers

with higher efficacy to allow the administration of lower total doses of PTX, and platforms for delivery of PTX that improve targeting to malignant tissues[18-27].

Liposomes are promising and versatile carriers (vectors) of drugs in therapeutic applications due to their biocompatibility and ability to sequester a wide range of molecules. These payloads include hydrophilic drugs and nucleic acids (NAs, e.g., DNA, siRNA and mRNA) in addition to hydrophobic drugs[5,28-36]. A prominent example of a liposomal carrier of a hydrophobic drug is Doxil®,[37] the formulation of another commonly used chemotherapeutic agent (doxorubicin). Doxil allows increased doxorubicin dosing because it reduces the cardiotoxicity associated with the administration of the free drug. However, the specific chemical properties of doxorubicin enable loading of the liposomes by a process that is not transferable to most other drugs including PTX.

Cationic liposomes (CLs; consisting of mixtures of cationic (or ionizable) and neutral lipids) in particular are prevalent nonviral vectors for the delivery of therapeutic NAs as recently demonstrated with the mRNA vaccines against COVID-19[38-41]. However, they are also suitable carriers for hydrophobic drugs. A cationic lipid-based carrier of PTX that has advanced to phase III clinical trials is EndoTAG®-1, which consists of DOTAP/DOPC CLs with 3 mol% PTX[19,25,35,42] (DOTAP, *N*-[2,3-dioleoyloxy-1-propyl]-trimethylammonium chloride, is a univalent cationic lipid; DOPC, 1,2-dioleoyl-*sn*-glycerophospho-choline, is a naturally occurring neutral phospholipid.) EndoTAG-1 has been shown to target tumor endothelial cells in solid tumors via nonspecific electrostatic interactions with cell surface anionic sulfated proteoglycans[36,42-46]. Unlike NAs and hydrophilic drugs (as well as doxorubicin nanocrystals in Doxil), which are packed in the aqueous medium between membranes, PTX is solubilized within the hydrophobic region of the membrane of lipid-based carriers.

The properties of lipid-based vectors of PTX can be tuned and improved in a variety of ways. By chemically modifying the constituent lipids, in particular the tails which interact with and solubilize PTX, the solubility of PTX and thus the drug loading can be increased markedly[47] beyond the 3 mol% solubility "limit"[48] of the PTX content that has been a limitation for most efficacy studies and clinical trials to

date[19,25,35,42,44]. Lipid carriers also offer the advantage of enabling future targeted delivery *in vivo* (e.g. via cyclic homing peptides attached to poly(ethylene glycol)-lipids (PEG-lipids) coating the CL vectors[49,50]).

In addition, modification of the lipids and the lipid composition of CL vectors can drive structural transitions[29,51-55], including the spontaneous formation of PEGylated micelles (discs, cylinders and spheroids observed in cryogenic TEM) coexisting with vesicles.[56,57]

For example, a recent publication reported that PEGylation of CL-based vectors of PTX via the addition of PEG-lipids strongly reduces the average size of the CLs[57]. At sufficiently high concentration (with the PEG chains in the brush regime), the PEG-lipid component provides steric stabilization that suppresses the aggregation of non-PEGylated CLs in cell culture medium (with ionic strength≈150 mM, comparable to conditions *in vivo*). Simultaneously, PEGylation gives rise to a proliferation of nanometer-scale disc-shaped bicelles (lipid nanodiscs) (Figure 1). This unexpected formation of nanodiscs at concentrations of the PEG-coat in the vicinity of the mushroom-brush transition regime was discovered by cryogenic TEM of PEGylated CLs[57].

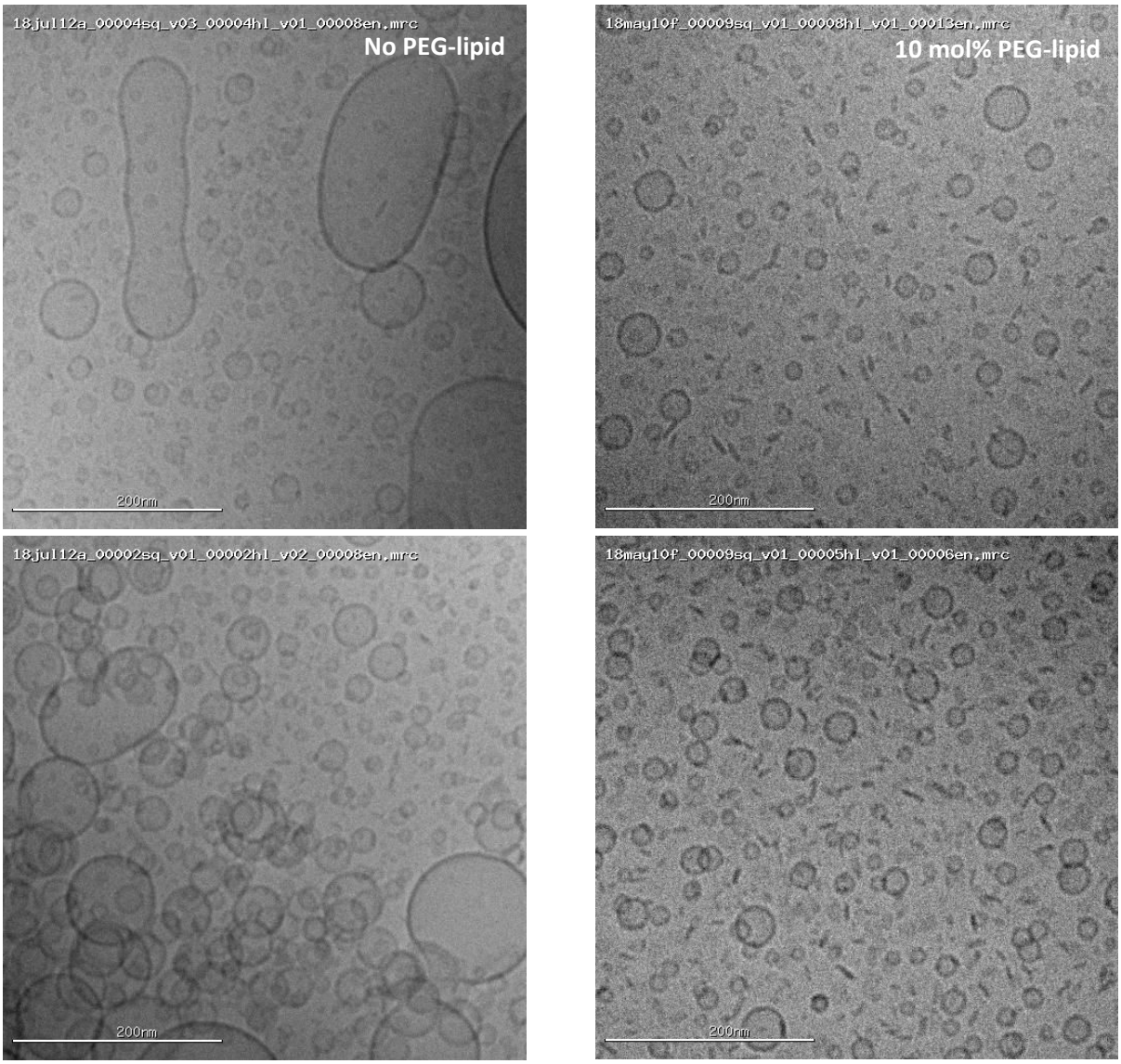

Figure 1. Cryogenic TEM images of CL-based vectors of PTX with and without PEGylation. **(Left)** A sample of sonicated liposomes at the EndoTAG-1 compositon (DOTAP/DOPC/PTX=50/47/3 molar ratio), exhibiting both larger and smaller vesicles with few discs. **(Right)** A sample of sonicated CL-based PTX vectors with 10 mol% PEG2K-lipid (DOTAP/DOPC/PEG2K-lipid/PTX=50/37/10/3 molar ratio), lacking vesicles above ~50 nm in size and showing a large number or very small vesicles and lipid discs.

The breakup of large liposomes into nanodiscs and very small vesicles strongly increases the solution entropy. However, an enthalpic elastic cost is incurred by the creation of membrane areas with high curvature (i.e., the surfaces of spherical or cylindrical micelles and the edges of discs). In the case of the discs seen in Figure 1, this enthalpy cost is lowered to below the overall gain in solution entropy by a

segregation of cone-shaped PEG-lipids (with spontaneous curvature C_0>0, Figure 2) into the high-curvature edges of the discs which stabilizes them. (C_0, the spontaneous (i.e., preferred) curvature of the membrane, is determined by the "shape" of the constituting lipid molecules, which is set by the size of the area of the lipid headgroup relative to the size of the area of the tails[58-61] [Figure 2].) Without such lipid segregation or lateral phase separation within the membrane (which is associated with its own cost in entropy for the segregating lipids), the increase in membrane curvature stemming from the addition of cone-shaped lipids such as PEG-lipids or highly charged lipids results in a reduction of the size of the lipid assemblies. The size (radius) of the assemblies will be of order of $1/C_0$, because the membrane curvature, C, of lipid assemblies (as measured in experiments) is typically maintained close to C_0 to avoid an elastic energy penalty[62-64].

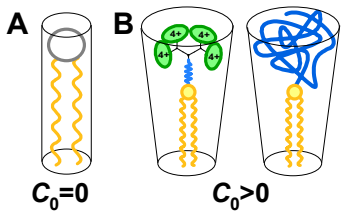

Figure 2. (A,B) Two common shapes of lipid molecules which result in membrane spontaneous curvature C_0=0 (A, e.g. DOPC; cylindrical shape yielding flat bilayers), and C_0>0 (B, e.g. PEG-lipids and highly charged lipids; cone shape yielding micellar monolayer assemblies or high curvature bilayers). The magnitude of C0 strongly affects the curvature of the lipid assembly and thus its size.

Importantly, the PEGylated lipid vectors consisting of coexisting PEGylated CLs_{PTX} and PTX-containing nanodiscs ($nanodiscs_{PTX}$), with PEG chains in the brush state, showed a significant enhancement of cellular uptake and cytotoxicity (i.e., efficacy) against human cancer cells *in vitro* compared to formulations similar to the benchmark EndoTAG-1, with cell viability decreasing in a PEG concentration-dependent manner[57]. This suggests that the size, stabilization, and possibly shape of the PEGylated lipid vector promotes cell uptake and thereby PTX delivery through different size-dependent endocytic pathways.

The finding that incorporating PEG-lipids yields CL carriers of PTX with stable micellar structures and high efficacy *in vitro* invited development of functionalized liposomes for *in vivo* delivery applications. Thus, we selected a series of PEGylated CL vectors of PTX for studies of biodistribution and cytotoxic activity *in vivo* to further assess their potential for therapeutic applications.

We determined the blood half-life *in vivo* and studied the tumor accumulation and apoptotic effect of the different PEGylated cationic lipid formulations of PTX in triple-negative breast tumors in mice. These studies showed that, compared to vectors with 2 and 5 mol% PEG5K-lipid, lipid nanoparticle vectors containing 10 mol% of PEG5K-lipid, consisting of a coexisting mixture of PEGylated CLs_{PTX} and $nanodiscs_{PTX}$ with the PEG chains in the extended brush conformation, possessed longer half-life, resulted in significantly higher tumor accumulation, and increased the activation of proapoptotic caspase-3 after systemic administration.

Materials and Methods

Samples for cryogenic TEM were prepared and imaged as described previously[57].

Materials

A stock solution of carboxyfluorescein-labeled DOPE (1,2-dioleoyl-*sn*-glycero-3-phosphoethanolamine-N-(carboxyfluorescein), DOPE-FAM) in chloroform was purchased from Avanti Polar Lipids. Other lipid stock solutions were prepared by dissolving DOPE-PEG5000, DOTAP, and DOPC, purchased from Avanti Polar Lipids, in chloroform at 3.64, 41.93, and 31.8 mM, respectively. A stock solution of PTX in chloroform was prepared by dissolving solid PTX (Biotang Inc.) in chloroform at 10 mM.

Liposome preparation

Mixed solutions of lipid and PTX were prepared in chloroform:methanol (3:1, v/v) in small glass vials at a total concentration of 1 mM for PTX solubility, biodistribution, and caspase activity experiments and 16.75 mM for lipid solubility experiments. The chloroform:methanol solvent was evaporated for 10 min under a nitrogen stream and the lipid was further dried in a vacuum for 16 h. The resultant film was resuspended in PBS to 1 mM for PTX solubility, biodistribution, and caspase activity experiments or

67 mM for lipid solubility experiments. This suspension was sonicated for 7 min with a tip sonicator (30 W output) to form small unilamellar vesicles.

DIC microscopy

For PTX solubility experiments, 2 μL each of cationic lipid formulations containing 10 mol% PEG5K-lipid and 2, 2.5, or 3 mol% PTX were placed on glass microscope slides and covered by coverslips secured by parafilm cutouts. All remaining samples were incubated for 20 h at room temperature before 2 μL were again taken for imaging. For lipid solubility experiments, 2 μL each of samples of formulations with 2, 5, and 10 mol% PEG5K-lipid were placed on glass microscope slides and again covered by coverslips secured by parafilm cutouts. All slides were imaged at 40× magnification on an inverted Ti2-E (Nikon) microscope.

Determination of the half-life of PEGylated paclitaxel containing cationic liposome vectors

Eight week-old immunocompetent female Balb/C mice were i.v. injected with 100 μL of PEGylated cationic liposome formulations of PTX containing 2, 5, or 10 mol% PEG5K-lipid. After 15, 30, 60, 180, 360 and 1440 min circulation, 5 μL of blood was extracted from the tail and mixed with 50 μL of saline phosphate buffer pH 7.4 (PBS) with heparin at 4 °C. The samples were centrifuged at 300 *g* at 4 °C for 5 min. The fluorescence of the supernatant was measured at 490 nm/535 nm (excitation/emission) using the Victor X5 Multilabel Microplate Reader (Perkin Elmer, USA). The data were fitted to a curve using a biexponential decay formula, to obtain the half-life of the PEGylated formulations.

Detection of tumor accumulation of PEGylated paclitaxel containing cationic liposome vectors and cleaved caspase-3 immunostaining

The animal experiments were performed according to protocols approved by Estonian Ministry of Agriculture, Committee of Animal Experimentation (projects #159 and #160). Triple-negative breast cancer cells (10^6 4T1 cells in 50 μL of PBS) were orthotopically injected into mammary gland of 8 week-old immunocompetent female Balb/C mice. One week later, 100 μL of PEGylated cationic liposome formulations of PTX were intravenously administered into the tail vein and 24 h later, mice were anesthetized, perfused with PBS and the tumor and organs were excised and kept in 4%

paraformaldehyde (PFA) solution in PBS at 4 °C overnight. PFA-fixed tissues were washed and immersed in PBS for 1 h at room temperature (RT). Then, the tissues were incubated in 15% sucrose solution in PBS at 4 °C overnight. The following day, the 15% solution was replaced with 30% sucrose solution in PBS and kept overnight at 4 °C. The tissues were frozen down in OCT (optimal cutting temperature) and cryo-sectioned at 20 µm. The sections were dried at RT for 1 h, permeabilized with PBS containing 0.2% Triton-X for 15 min, washed with PBS containing 0.05% Tween-20 (PBST), and blocked with PBST containing 5% bovine serum albumin (BSA), 5% fetal bovine serum (FBS), and 5% goat serum for 1 h. The tissue sections were incubated at 4 °C overnight with rat anti-mouse CD31 (cat. no. 553370, BD Biosciences) and rabbit anti-cleaved Caspase-3 (#9661, Cell Signaling Technology) as primary antibodies in blocking buffer diluted 1 in 5 in PBST (antibody dilution 1/200 and 1/400 respectively). Alexa 647-conjugated goat anti-rabbit IgG (cat. no. A21245, Thermo Fischer Scientific) and Alexa 546-conjugated goat anti-rat IgG (cat. no. A11081, Thermo Fischer Scientific) were used as secondary antibodies (antibody dilution 1/300). The slides were incubated with the secondary antibodies for 2 h at RT. The sections were washed with PBST and PBS, and the nuclei were stained with 1 µg/mL DAPI in PBS for 5 min. Stained slides were mounted with mounting medium and sealed with nail polish. The tissues were imaged using a fluorescence confocal microscope (FV1200MPE, Olympus), and the image analyzed using the Olympus FluoView Ver.4.2a Viewer program. To quantify the intensity of the FAM signal from PEGylated lipid vectors and cleaved caspase-3, confocal images were analyzed using ImageJ. Two to six random areas per tumor were chosen and this was repeated in three tumor-bearing mice for each group.

Statistical tests

The statistical analyses were performed with Statistica 8 software (StatSoft, USA) using the one-way ANOVA and Fisher LSD tests.

Results and Discussion

PTX membrane solubility in PEGylated liposomes

As mentioned in the introduction, it is essential for the efficacy of PTX-loaded CLs that PTX remains soluble in the membrane. We previously found that the membrane solubility of PTX is slightly lower in PEGylated CLs than in bare CLs[48,57]. To determine the optimal PTX content for the CLs employed in the current study, we assessed the solubility of PTX in CLs containing 10 mol% PEG5K-lipid, the highest PEG-lipid content used. The formation of therapeutically inert PTX crystals, due to PTX self-association in the membrane and subsequent phase separation, is an indicator of PTX insolubility[48,65]. To measure PTX solubility in PEG-CL membranes, we monitored PTX crystal formation with DIC microscopy[48,57]. Representative DIC micrographs of sonicated CLs containing 10 mol% PEG5K-lipid and 2 to 3 mol% PTX are displayed in Figure 3. Insoluble PTX formed crystals in PEG-CL samples with 3 mol% PTX after 20 hours at room temperature (Figure 3, top right panel), while PTX remained solubilized in samples with 2 and 2.5 mol% PTX (Figure 3, middle and bottom right panels). Thus, we chose 2.5 mol% as the PTX concentration for formulations for the *in vivo* efficacy experiments where a maximal loading of PTX is desirable and 2 mol% PTX, where PTX remains soluble for days, for biodistribution experiments.

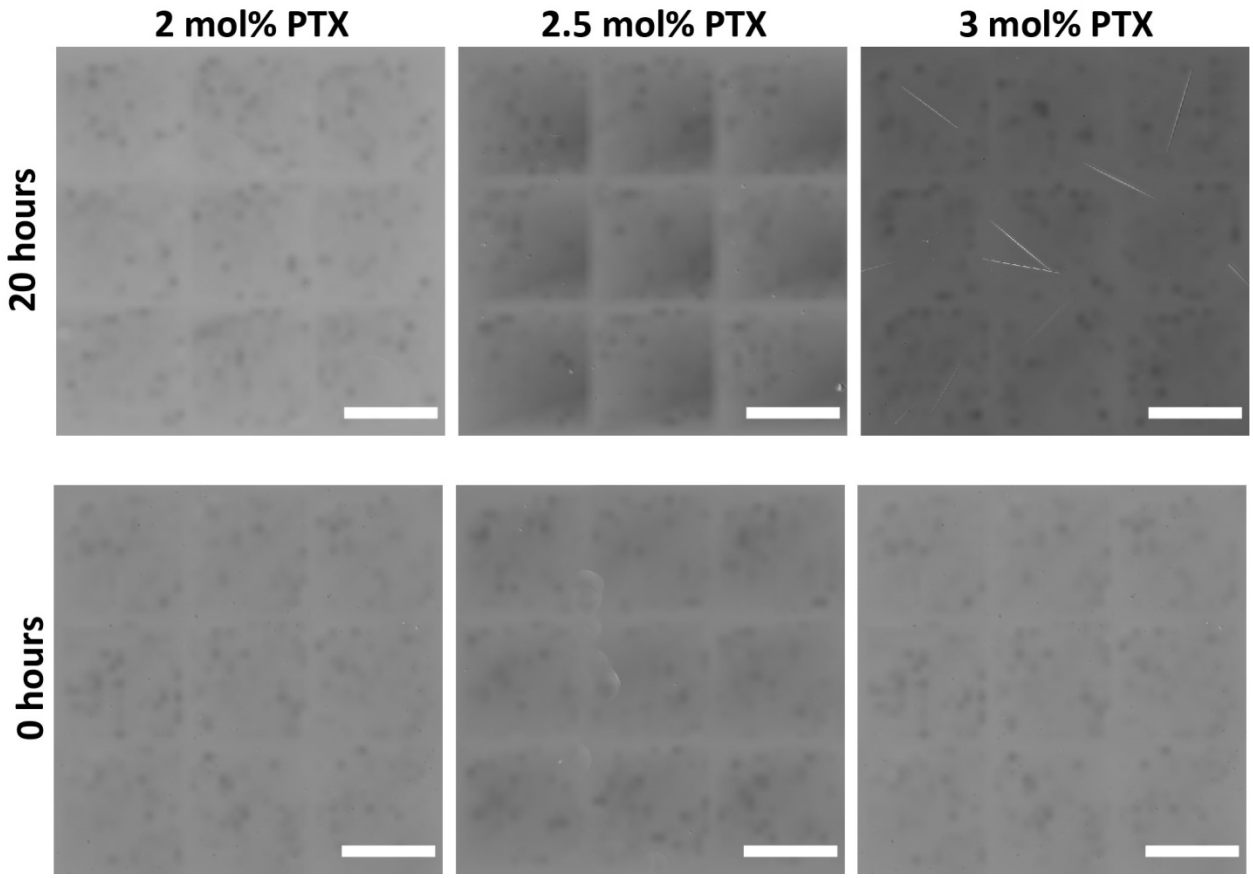

Figure 3. Solubility of PTX in PEGylated CLs as a function of drug loading. The figure displays DIC micrographs of sonicated CLs containing 10 mol% PEG5K-lipid, loaded with 2 (left column), 2.5 (center column), and 3 (right column) mol% PTX, immediately (bottom row) and 20 h (top row) after preparation by resuspension in PBS. PTX crystals were not present in any liposome sample immediately following resuspension but had formed 20 hours after resuspension for CLs containing 3 mol% PTX (top right panel) but not 2 or 2.5 mol% PTX. CL composition: PEG5K-lipid:DOTAP:DOPC:PTX=10:50:40–x_{PTX}:x_{PTX} molar ratio, with x_{PTX} the PTX content in mol%). Scale bars: 200 μm.

PEGylation increases cationic liposome solublity at high lipid concentrations

For studies of therapeutic efficacy, PTX-loaded CLs must be prepared at total lipid concentrations of 50 mg/mL or greater to achieve sufficiently high PTX dosages[66,67]. We thus prepared sonicated CL suspensions at a total lipid concentration of 50 mg/mL for formulations with varying degrees of PEGylation. At this high concentration, formulations containing 2 mol% PEG5K-lipid spontaneously formed giant multilamellar structures, greater than ~100 μm in size, that are visible in DIC microscopy (Figure 4, left panel). Consistent with our previous findings that PEG-lipid incorporation stabilizes small

unilamellar vesicles and bicelles and suppresses the formation of larger CL structures[57], such large structures were not found in CLs containing 5 and 10 mol% PEG5K-lipid (Figure 4, center and right panels). However, samples with 5 mol% PEG5K-lipid produced some structures which were elongated in contrast to the spherical morphologies of DIC-detectable objects in samples with 10 mol% PEG5K-lipid. Note that the small vesicles and discs visible in cryogenic TEM are undetectable by optical microscopy due to their small size. The giant multilamellar structures observed in CLs with 2 mol% PEG5K-lipid are likely prohibitive for their use in applications *in vivo*, and only the formulations with higher PEG5K-lipid content were chosen to investigate their therapeutic efficacy.

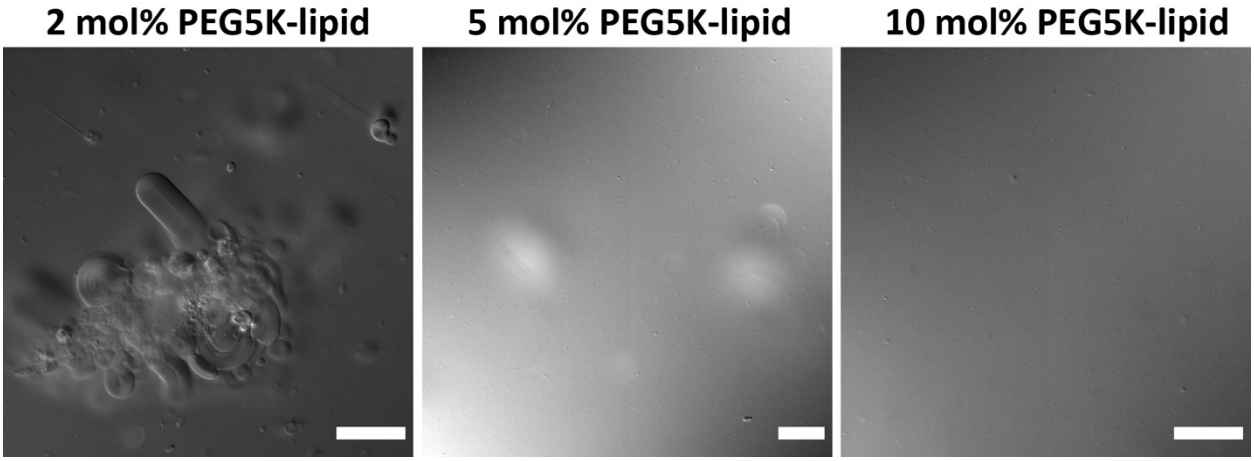

Figure 4. Solubility of lipid formulations as a function of PEG5K-lipid content. DIC microscopy images from sonicated 2, 5, and 10 mol% PEG5K-lipid containing liposomes 2 hours after rehydration at 67 mM in PBS. Few aggregates or particles greater than ~5 µm were observed in liposomes containing 5 and 10 mol% PEG5K-lipid (center and right panels), with the 10 mol% PEG5K-lipid formulation showing the least number of aggregates (i.e. providing strong steric stabilization of lipid particles). In contrast, many aggregates greater than ~5 µm and some greater than 50 µm were present in liposomes containing 2 mol% PEG5K-lipid (left panel). Liposome molar composition: PEG5K-lipid, DOTAP, DOPC, PTX ($x_{PEG5K\text{-}lipid}$:50:48-$x_{PEG5K\text{-}lipid}$:2). Scale bars are 50 µm.

Increased PEGylation of PTX-loaded cationic liposome vectors extends the blood half-life

To assess the potential of PEGylated cationic liposome vectors containing PTX for applications *in vivo*, we first studied the effect of differential PEGylation (at 2, 5, or 10 mol% of PEG5K-lipid) on the blood clearance of systemic FAM-labeled lipid vectors (at low concentration) in immunocompetent healthy

mice. The molar composition of the formulations was PEG5K-lipid:DOTAP:DOPC:PTX=$x_{PEG5K-lipid}$:50:48-$x_{PEG5K-lipid}$:2. Whereas the plasma half-life of the formulations containing 2 and 5 mol% of PEG5K-lipid was similar (39 and 34 min respectively), the half-life of the formulation with 10% of PEG-lipid was extended to 90 min (Figure 5). This increase in plasma half-life at 10 mol% PEG was likely due to escape of the surveillance by reticuloendothelial system due to increase in "stealth" properties and/or in the CL shape changes. Efficiency of nanoparticle uptake by phagocytic cells is known to be influenced by shape of the particles, a phenomenon attributed to shape and aspect ratio-dependent activation of different endocytic pathways[68].

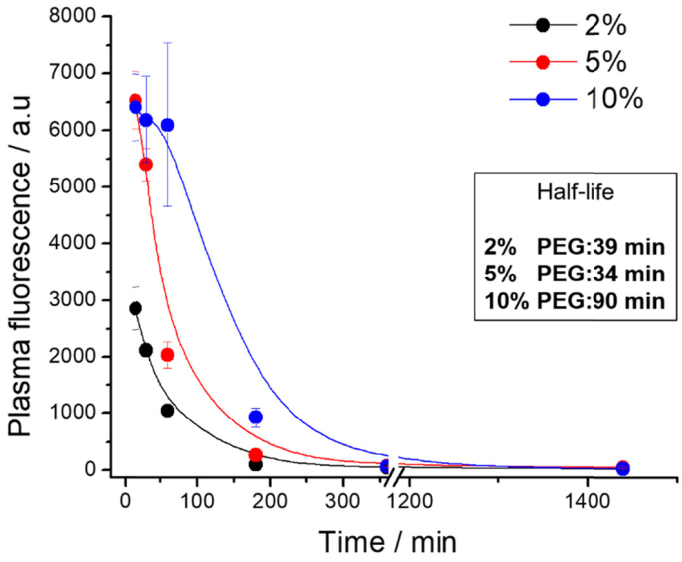

Figure 5. The plasma half-life of PTX-loaded cationic liposome vectors increases with PEGylation. A: Plasma half-life of intravenously administered FAM-labeled PEGylated PTX-loaded cationic liposome vectors containing 2, 5 and 10 mol% of PEG5K-lipid in healthy Balb/c mice. Mice (N=3) were intravenously injected with indicated formulations, blood samples were collected at different time points and the fluorescence of plasma was measured. The values were fitted using a biexponential decay formula, to obtain the half-life. Error bars indicate the standard error of the mean (±SEM).

Increased PEGylation of PTX-loaded cationic liposome vectors, driving the PEG chains in the extended brush state, potentiates their tumor accumulation and proapoptotic activity

We next studied the effects of differential PEGylation of PTX-loaded cationic liposome vectors on biodistribution and tumor accumulation. Mice bearing 50–75 mm^3 orthotopic 4T1 triple negative breast

cancer (TNBC) lesions were i.v. injected with FAM-labeled PTX-loaded cationic liposome formulations at 2, 5 and 10 mol% of PEG5K-lipid. Twenty-four hours later, the tumors were collected, cryo-sectioned, and imaged for FAM fluorescence by fluorescence confocal microscopy (Figure 6A). The level of PEGylated lipid vectors in the tumor increased with the PEG5K-lipid content: the tumor accumulation of the lipid formulations containing 10 mol% of PEG5K-lipid (PEGylated CLs_{PTX} and coexisting $nanodiscs_{PTX}$), with the brush conformation of PEG conferring steric stabilization, was 2-fold and 5-fold higher than that of the lipid formulations containing 5 and 2 mol% of PEG5K-lipid, respectively (Figure 6B). Moreover, the signal of the lipid formulation with 10% PEG5K-lipid did not colocalize with the blood vessels (red signal in Figure 6A), suggesting that the vector particles extravasated and reached the tumor parenchyma. These observations are in line with previous studies showing that a longer half-life increases the chances of passive accumulation of nanoparticles at the tumor site. We note that in the 5 mol% PEG5K-lipid formulation (also a coexisting mixture of PEGylated CLs_{PTX} and $nanodiscs_{PTX}$, but with a different ratio of the two structures compared to the 10 mol% PEG5K-lipid formulation), the PEG chains are in the mushroom state near transition to the brush conformation and offer lower levels of steric stabilization compared to the 10 mol% PEG5K-lipid formulation. The 2 mol% PEG5K-lipid formulation, with PEG chains in the mushroom regime far from the brush regime, is not sterically stabilized (consistent with DIC images in Figure 4).

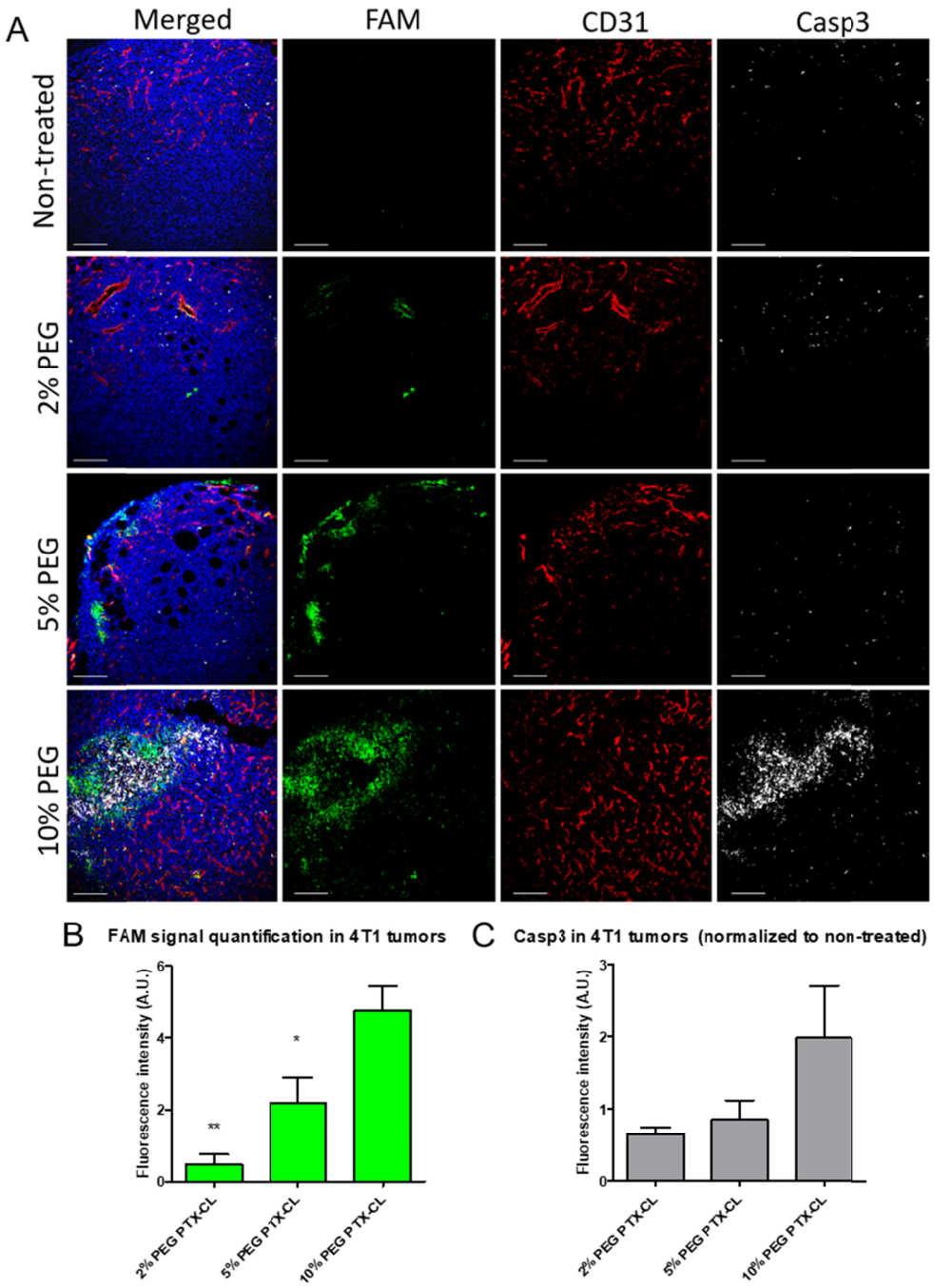

Figure 6. Increased content of PEG5K-lipid in PTX-loaded cationic liposome vectors potentiates accumulation in breast tumors and increases apoptotic cell death. A: Tumor homing and cell death of PEGylated CL_{PTX} vectors containing 2, 5, and 10 mol% PEG5K-lipid assessed by immunofluorescence microscopy. The different formulations were administered intravenously in 4T1 tumor-bearing mice; 24 h later the mice were perfused with PBS, tumors excised, cryo-sectioned, and immunostained for CD31 (blood vessels; red) and cleaved caspase-3 (white), and stained with DAPI nuclear counterstain (blue); the green signal represents the FAM fluorescence of the PEG-CL_{PTX}. Scale bar: 200 µM. **B and C:** FAM **(B)**

and **(C)** cleaved caspase-3 signal quantification normalized to non-treated tumors from panel A, from at least 3 different images from 3 different tumors per group. Error bars indicate the SEM, statistical test: ANOVA one way, Fisher LSD.

Next, we studied if the higher tumor 4T1 tumor accumulation of the lipid vector formulation with 10 mol% PEG5K-lipid (sterically stabilized PEGylated CLs_{PTX} and coexisting $nanodiscs_{PTX}$) translated into an enhanced *in vivo* anticancer efficacy. Tumors from animals treated with the PEGylated lipid vectors were stained for cleaved caspase-3, a marker of apoptotic cells. No increased signal of cleaved caspase-3 was observed in the tumors treated with lipid formulations containing 2 and 5 mol% PEG5K-lipid compared with the untreated tumors (Figure 6, parts A and C). In contrast, the tumors treated with lipid formulations containing 10 mol% of PEG5K-lipid (brush-state PEGylated CLs_{PTX} and coexisting $nanodiscs_{PTX}$) showed a 2-fold higher signal of cleaved caspase-3 (Figure 6C), although this difference did not reach statistical significance, possibly due to the low PTX dose administered and the short time point used to observe the effect of PTX. Importantly, the signal for cleaved caspase-3 was observed in areas overlapping or adjacent to the fluorescent signal of the lipid formulation with 10 mol% PEG5K-lipid (Figure 6A), suggesting that this formulation was able to efficiently release PTX and trigger cell apoptosis.

Acknowledgements

This research study was supported by the National Institutes of Health under Award R01GM130769 (CRS,KKE,WF, mechanistic studies on developing lipid nanoparticles for drug delivery), by the European Regional Development Fund (TT, Project No. 2014-2020.4.01.15-0012), the Estonian Research Council (TT, grants PRG230 and EAG79; PDS, PSG38; LSG, MOBJD11), and the Spanish Ministry of Science (PDS, RYC2020-028754-I). Partial support was provided by the US National Science Foundation (NSF) under Award DMR-1807327 (CRS, kinetic phase behavior of cationic vesicles with incorporated hydrophobic molecules).

References

(1) Wani, M. C.; Taylor, H. L.; Wall, M. E.; Coggon, P.; McPhail, A. T. Plant antitumor agents. VI. Isolation and structure of taxol, a novel antileukemic and antitumor agent from Taxus brevifolia. *J. Am. Chem. Soc.* **1971**, *93*, 2325-2327.

(2) Jordan, M. A.; Wilson, L. Microtubules as a target for anticancer drugs. *Nat. Rev. Cancer* **2004**, *4*, 253-265.

(3) Weaver, B. A. How Taxol/paclitaxel kills cancer cells. *Mol. Biol. Cell* **2014**, *25*, 2677-2681.

(4) Rowinsky , E. K.; Donehower , R. C. Paclitaxel (Taxol). *N. Engl. J. Med.* **1995**, *332*, 1004-1014.

(5) Sofias, A. M.; Dunne, M.; Storm, G.; Allen, C. The battle of "nano" paclitaxel. *Adv. Drug Delivery Rev.* **2017**, *122*, 20-30.

(6) Markman, M.; Mekhail, T. M. Paclitaxel in cancer therapy. *Expert Opin. Pharmacother.* **2002**, *3*, 755-766.

(7) Ramalingam, S.; Belani, C. P. Paclitaxel for non-small cell lung cancer. *Expert Opin. Pharmacother.* **2004**, *5*, 1771-1780.

(8) Hironaka, S.; Zenda, S.; Boku, N.; Fukutomi, A.; Yoshino, T.; Onozawa, Y. Weekly paclitaxel as second-line chemotherapy for advanced or recurrent gastric cancer. *Gastric Cancer* **2006**, *9*, 14-18.

(9) Sakamoto, J.; Matsui, T.; Kodera, Y. Paclitaxel chemotherapy for the treatment of gastric cancer. *Gastric Cancer* **2009**, *12*, 69-78.

(10) Moxley, K. M.; McMeekin, D. S. Endometrial Carcinoma: A Review of Chemotherapy, Drug Resistance, and the Search for New Agents. *Oncologist* **2010**, *15*, 1026-1033.

(11) World Health Organization WHO Model Lists of Essential Medicines. http://www.who.int/medicines/publications/essentialmedicines/en/ (accessed Mar 16, 2021),

(12) Dranitsaris, G.; Yu, B.; Wang, L.; Sun, W.; Zhou, Y.; King, J.; Kaura, S.; Zhang, A.; Yuan, P. Abraxane® versus Taxol® for patients with advanced breast cancer: A prospective time and motion analysis from a Chinese health care perspective. *J. Oncol. Pharm. Pract.* **2016**, *22*, 205-211.

(13) Rugo, H. S.; Barry, W. T.; Moreno-Aspitia, A.; Lyss, A. P.; Cirrincione, C.; Leung, E.; Mayer, E. L.; Naughton, M.; Toppmeyer, D.; Carey, L. A.; Perez, E. A.; Hudis, C.; Winer, E. P. Randomized Phase III Trial of Paclitaxel Once Per Week Compared With Nanoparticle Albumin-Bound Nab-Paclitaxel Once Per Week or Ixabepilone With Bevacizumab As First-Line Chemotherapy for Locally Recurrent or Metastatic Breast Cancer: CALGB 40502/NCCTG N063H (Alliance). *J. Clin. Oncol.* **2015**, *33*, 2361-2369.

(14) Gradishar, W. J.; Tjulandin, S.; Davidson, N.; Shaw, H.; Desai, N.; Bhar, P.; Hawkins, M.; O'Shaughnessy, J. Phase III Trial of Nanoparticle Albumin-Bound Paclitaxel Compared With Polyethylated Castor Oil–Based Paclitaxel in Women With Breast Cancer. *J. Clin. Oncol.* **2005**, *23*, 7794-7803.

(15) Weiss, R. B.; Donehower, R. C.; Wiernik, P. H.; Ohnuma, T.; Gralla, R. J.; Trump, D. L.; Jr, J. R. B.; Echo, D. A. V.; Hoff, D. D. V.; Leyland-Jones, B. Hypersensitivity reactions from taxol. *J. Clin. Oncol.* **1990**, *8*, 1263-1268.

(16) Dorr, R. T. Pharmacology and Toxicology of Cremophor EL Diluent. *Ann. Pharmacother.* **1994**, *28*, S11-S14.

(17) Gelderblom, H.; Verweij, J.; Nooter, K.; Sparreboom, A. Cremophor EL: the drawbacks and advantages of vehicle selection for drug formulation. *Eur. J. Cancer* **2001**, *37*, 1590-1598.

(18) Hong, S.-S.; Choi, J. Y.; Kim, J. O.; Lee, M.-K.; Kim, S. H.; Lim, S.-J. Development of paclitaxel-loaded liposomal nanocarrier stabilized by triglyceride incorporation. *Int. J. Nanomed.* **2016**, *11*, 4465-4477.

(19) Fetterly, G. J.; Straubinger, R. M. Pharmacokinetics of paclitaxel-containing liposomes in rats. *AAPS PharmSci* **2003**, *5*, E32.

(20) Sharma, A.; Mayhew, E.; Straubinger, R. M. Antitumor Effect of Taxol-containing Liposomes in a Taxol-resistant Murine Tumor Model. *Cancer Res.* **1993**, *53*, 5877-5881.

(21) Zhou, R.; Mazurchuk, R. V.; Tamburlin, J. H.; Harrold, J. M.; Mager, D. E.; Straubinger, R. M. Differential Pharmacodynamic Effects of Paclitaxel Formulations in an Intracranial Rat Brain Tumor Model. *J. Pharmacol. Exp. Ther.* **2010**, *332*, 479-488.

(22) Xu, X.; Wang, L.; Xu, H.-Q.; Huang, X.-E.; Qian, Y.-D.; Xiang, J. Clinical comparison between paclitaxel liposome (Lipusu®) and paclitaxel for treatment of patients with metastatic gastric cancer. *Asian Pac. J. Cancer Prev.* **2013**, *14*, 2591-2594.

(23) Wang, H.; Cheng, G.; Du, Y.; Ye, L.; Chen, W.; Zhang, L.; Wang, T.; Tian, J.; Fu, F. Hypersensitivity reaction studies of a polyethoxylated castor oil-free, liposome-based alternative paclitaxel formulation. *Mol. Med. Rep.* **2013**, *7*, 947-952.

(24) Zhang, J. A.; Anyarambhatla, G.; Ma, L.; Ugwu, S.; Xuan, T.; Sardone, T.; Ahmad, I. Development and characterization of a novel Cremophor® EL free liposome-based paclitaxel (LEP-ETU) formulation. *Eur. J. Pharm. Biopharm.* **2005**, *59*, 177-187.

(25) Sharma, A.; Sharma, U. S.; Straubinger, R. M. Paclitaxel-liposomes for intracavitary therapy of intraperitoneal P388 leukemia. *Cancer Lett.* **1996**, *107*, 265-272.

(26) Simón-Gracia, L.; Hunt, H.; Scodeller, P. D.; Gaitzsch, J.; Braun, G. B.; Willmore, A.-M. A.; Ruoslahti, E.; Battaglia, G.; Teesalu, T. Paclitaxel-Loaded Polymersomes for Enhanced Intraperitoneal Chemotherapy. *Mol. Cancer Ther.* **2016**, *15*, 670-679.

(27) Simón-Gracia, L.; Hunt, H.; Scodeller, P.; Gaitzsch, J.; Kotamraju, V. R.; Sugahara, K. N.; Tammik, O.; Ruoslahti, E.; Battaglia, G.; Teesalu, T. iRGD peptide conjugation potentiates intraperitoneal tumor delivery of paclitaxel with polymersomes. *Biomaterials* **2016**, *104*, 247-257.

(28) Safinya, C. R.; Ewert, K. K.; Majzoub, R. N.; Leal, C. Cationic liposome-nucleic acid complexes for gene delivery and gene silencing. *New J. Chem.* **2014**, *38*, 5164-5172.

(29) Ewert, K. K.; Scodeller, P.; Simón-Gracia, L.; Steffes, V. M.; Wonder, E. A.; Teesalu, T.; Safinya, C. R. Cationic Liposomes as Vectors for Nucleic Acid and Hydrophobic Drug Therapeutics. *Pharmaceutics* **2021**, *13*, 1365.

(30) Torchilin, V. P. Recent advances with liposomes as pharmaceutical carriers. *Nat. Rev. Drug Discovery* **2005**, *4*, 145.

(31) Allen, T. M.; Cullis, P. R. Liposomal drug delivery systems: From concept to clinical applications. *Adv. Drug Delivery Rev.* **2013**, *65*, 36-48.

(32) Witzigmann, D.; Kulkarni, J. A.; Leung, J.; Chen, S.; Cullis, P. R.; van der Meel, R. Lipid nanoparticle technology for therapeutic gene regulation in the liver. *Adv. Drug Delivery Rev.* **2020**, *159*, 344-363.

(33) Kulkarni, J. A.; Witzigmann, D.; Chen, S.; Cullis, P. R.; van der Meel, R. Lipid Nanoparticle Technology for Clinical Translation of siRNA Therapeutics. *Acc. Chem. Res.* **2019**, *52*, 2435-2444.

(34) Sercombe, L.; Veerati, T.; Moheimani, F.; Wu, S. Y.; Sood, A. K.; Hua, S. Advances and Challenges of Liposome Assisted Drug Delivery. *Front. Pharmacol.* **2015**, *6*, 286.

(35) Koudelka, Š.; Turánek, J. Liposomal paclitaxel formulations. *J. Controlled Release* **2012**, *163*, 322-334.

(36) Campbell, R. B.; Ying, B.; Kuesters, G. M.; Hemphill, R. Fighting cancer: From the bench to bedside using second generation cationic liposomal therapeutics. *J. Pharm. Sci.* **2009**, *98*, 411-429.

(37) Barenholz, Y. Doxil® — The first FDA-approved nano-drug: Lessons learned. *J. Controlled Release* **2012**, *160*, 117-134.

(38) Mulligan, M. J.; Lyke, K. E.; Kitchin, N.; Absalon, J.; Gurtman, A.; Lockhart, S.; Neuzil, K.; Raabe, V.; Bailey, R.; Swanson, K. A.; Li, P.; Koury, K.; Kalina, W.; Cooper, D.; Fontes-Garfias, C.; Shi, P.-Y.; Türeci, Ö.; Tompkins, K. R.; Walsh, E. E.; Frenck, R.; Falsey, A. R.; Dormitzer, P. R.; Gruber, W. C.; Şahin, U.; Jansen, K. U. Phase I/II study of COVID-19 RNA vaccine BNT162b1 in adults. *Nature* **2020**, *586*, 589-593.

(39) Polack, F. P.; Thomas, S. J.; Kitchin, N.; Absalon, J.; Gurtman, A.; Lockhart, S.; Perez, J. L.; Pérez Marc, G.; Moreira, E. D.; Zerbini, C.; Bailey, R.; Swanson, K. A.; Roychoudhury, S.; Koury, K.; Li, P.; Kalina, W. V.; Cooper, D.; Frenck, R. W.; Hammitt, L. L.; Türeci, Ö.; Nell, H.; Schaefer, A.; Ünal, S.; Tresnan, D. B.; Mather, S.; Dormitzer, P. R.; Şahin, U.; Jansen, K. U.; Gruber, W. C. Safety and Efficacy of the BNT162b2 mRNA Covid-19 Vaccine. *N. Engl. J. Med.* **2020**, *383*, 2603-2615.

(40) Jackson, L. A.; Anderson, E. J.; Rouphael, N. G.; Roberts, P. C.; Makhene, M.; Coler, R. N.; McCullough, M. P.; Chappell, J. D.; Denison, M. R.; Stevens, L. J.; Pruijssers, A. J.; McDermott, A.; Flach, B.; Doria-Rose, N. A.; Corbett, K. S.; Morabito, K. M.; O'Dell, S.; Schmidt, S. D.; Swanson, P. A.; Padilla, M.; Mascola, J. R.; Neuzil, K. M.; Bennett, H.; Sun, W.; Peters, E.; Makowski, M.; Albert, J.; Cross, K.; Buchanan, W.; Pikaart-Tautges, R.; Ledgerwood, J. E.; Graham, B. S.; Beigel, J. H. An mRNA Vaccine against SARS-CoV-2 — Preliminary Report. *N. Engl. J. Med.* **2020**, *383*, 1920-1931.

(41) Baden, L. R.; El Sahly, H. M.; Essink, B.; Kotloff, K.; Frey, S.; Novak, R.; Diemert, D.; Spector, S. A.; Rouphael, N.; Creech, C. B.; McGettigan, J.; Khetan, S.; Segall, N.; Solis, J.; Brosz, A.; Fierro, C.; Schwartz, H.; Neuzil, K.; Corey, L.; Gilbert, P.; Janes, H.; Follmann, D.; Marovich, M.; Mascola, J.; Polakowski, L.; Ledgerwood, J.; Graham, B. S.; Bennett, H.; Pajon, R.; Knightly, C.; Leav, B.; Deng, W.; Zhou, H.; Han, S.; Ivarsson, M.; Miller, J.; Zaks, T. Efficacy and Safety of the mRNA-1273 SARS-CoV-2 Vaccine. *N. Engl. J. Med.* **2020**, *384*, 403-416.

(42) Fasol, U.; Frost, A.; Büchert, M.; Arends, J.; Fiedler, U.; Scharr, D.; Scheuenpflug, J.; Mross, K. Vascular and pharmacokinetic effects of EndoTAG-1 in patients with advanced cancer and liver metastasis. *Ann. Oncol.* **2012**, *23*, 1030-1036.

(43) Strieth, S.; Eichhorn, M. E.; Sauer, B.; Schulze, B.; Teifel, M.; Michaelis, U.; Dellian, M. Neovascular targeting chemotherapy: Encapsulation of paclitaxel in cationic liposomes impairs functional tumor microvasculature. *Int. J. Cancer* **2004**, *110*, 117-124.

(44) Strieth, S.; Nussbaum, C. F.; Eichhorn, M. E.; Fuhrmann, M.; Teifel, M.; Michaelis, U.; Berghaus, A.; Dellian, M. Tumor-selective vessel occlusions by platelets after vascular targeting chemotherapy using paclitaxel encapsulated in cationic liposomes. *Int. J. Cancer* **2008**, *122*, 452-460.

(45) Kunstfeld, R.; Wickenhauser, G.; Michaelis, U.; Teifel, M.; Umek, W.; Naujoks, K.; Wolff, K.; Petzelbauer, P. Paclitaxel Encapsulated in Cationic Liposomes Diminishes Tumor Angiogenesis and Melanoma Growth in a "Humanized" SCID Mouse Model. *J. Invest. Dermatol.* **2003**, *120*, 476-482.

(46) Schmitt-Sody, M.; Strieth, S.; Krasnici, S.; Sauer, B.; Schulze, B.; Teifel, M.; Michaelis, U.; Naujoks, K.; Dellian, M. Neovascular Targeting Therapy: Paclitaxel Encapsulated in Cationic Liposomes Improves Antitumoral Efficacy. *Clin. Cancer Res.* **2003**, *9*, 2335-2341.

(47) Zhen, Y.; Ewert, K. K.; Fisher, W. S.; Steffes, V. M.; Li, Y.; Safinya, C. R. Paclitaxel loading in cationic liposome vectors is enhanced by replacement of oleoyl with linoleoyl tails with distinct lipid shapes. *Sci. Rep.* **2021**, *11*, 7311.

(48) Steffes, V. M.; Murali, M. M.; Park, Y.; Fletcher, B. J.; Ewert, K. K.; Safinya, C. R. Distinct Solubility and Cytotoxicity Regimes of Paclitaxel-Loaded Cationic Liposomes at Low and High Drug Content Revealed by Kinetic Phase Behavior and Cancer Cell Viability Studies. *Biomaterials* **2017**, *145*, 242-255.

(49) Ewert, K. K.; Kotamraju, V. R.; Majzoub, R. N.; Steffes, V. M.; Wonder, E. A.; Teesalu, T.; Ruoslahti, E.; Safinya, C. R. Synthesis of linear and cyclic peptide–PEG–lipids for stabilization and targeting of cationic liposome–DNA complexes. *Bioorg. Med. Chem. Lett.* **2016**, *26*, 1618-1623.

(50) Wonder, E.; Simón-Gracia, L.; Scodeller, P.; Majzoub, R. N.; Kotamraju, V. R.; Ewert, K. K.; Teesalu, T.; Safinya, C. R. Competition of charge-mediated and specific binding by peptide-tagged cationic liposome–DNA nanoparticles in vitro and in vivo. *Biomaterials* **2018**, *166*, 52-63.

(51) Koltover, I.; Salditt, T.; Rädler, J. O.; Safinya, C. R. An inverted hexagonal phase of cationic liposome-DNA complexes related to DNA release and delivery. *Science* **1998**, *281*, 78-81.

(52) Ewert, K. K.; Evans, H. M.; Zidovska, A.; Bouxsein, N. F.; Ahmad, A.; Safinya, C. R. A columnar phase of dendritic lipid-based cationic liposome-DNA complexes for gene delivery: Hexagonally ordered cylindrical micelles embedded in a DNA honeycomb lattice. *J. Am. Chem. Soc.* **2006**, *128*, 3998-4006.

(53) Leal, C.; Bouxsein, N. F.; Ewert, K. K.; Safinya, C. R. Highly Efficient Gene Silencing Activity of siRNA Embedded in a Nanostructured Gyroid Cubic Lipid Matrix. *J. Am. Chem. Soc.* **2010**, *132*, 16841-16847.

(54) Zidovska, A.; Evans, H. M.; Ewert, K. K.; Quispe, J.; Carragher, B.; Potter, C. S.; Safinya, C. R. Liquid crystalline phases of dendritic lipid-DNA self-assemblies: Lamellar, hexagonal, and DNA bundles. *J. Phys. Chem. B* **2009**, *113*, 3694-3703.

(55) Safinya, C. R.; Ewert, K. K.; Li, Y.; Rädler, J. O., Cationic Liposomes as Spatial Organizers of Nucleic Acids in One, Two, and Three Dimensions: Liquid Crystal Phases with Applications in

Delivery and Bionanotechnology. In *Handbook of Lipid Membranes: Molecular, Functional, and Materials Aspects*, Safinya, C. R.; Rädler, J. O., Eds. CRC Press, Taylor & Francis Group: Boca Raton, 2021; pp 195-209.

(56) Majzoub, R. N.; Ewert, K. K.; Jacovetty, E. L.; Carragher, B.; Potter, C. S.; Li, Y.; Safinya, C. R. Patterned Threadlike Micelles and DNA-Tethered Nanoparticles: A Structural Study of PEGylated Cationic Liposome–DNA Assemblies. *Langmuir* **2015**, *31*, 7073-7083.

(57) Steffes, V. M.; Zhang, Z.; MacDonald, S.; Crowe, J.; Ewert, K. K.; Carragher, B.; Potter, C. S.; Safinya, C. R. PEGylation of Paclitaxel-Loaded Cationic Liposomes Drives Steric Stabilization of Bicelles and Vesicles thereby Enhancing Delivery and Cytotoxicity to Human Cancer Cells. *ACS Appl. Mater. Interfaces* **2020**, *12*, 151-162.

(58) Israelachvili, J. N.; Mitchell, D. J.; Ninham, B. W. Theory of self-assembly of hydrocarbon amphiphiles into micelles and bilayers. *J. Chem. Soc.-Faraday Trans. 2* **1976**, *72*, 1525-1568.

(59) Israelachvili, J. N.; Mitchell, D. J.; Ninham, B. W. Theory of self-assembly of lipid bilayers and vesicles. *Biochim. Biophys. Acta, Biomembr.* **1977**, *470*, 185-201.

(60) Israelachvili, J. N., *Intermolecular and Surface Forces*. 3rd ed.; Elsevier: Amsterdam, 2011.

(61) Seddon, J. M. Structure of the inverted hexagonal (HII) phase, and non-lamellar phase transitions of lipids. *Biochim. Biophys. Acta* **1990**, *1031*, 1-69.

(62) Helfrich, W. Z. Elastic Properties of Lipid Bilayers: Theory and Possible Experiments. *Z. Naturforsch., C: J. Biosci.* **1973**, *28*, 693-703.

(63) Lipowsky, R.; Sackmann, E., *Structure and Dynamics of Membranes*. Elsevier: Amsterdam, 1995; Vol. 1A.

(64) Safran, S. A., *Statistical thermodynamics of surfaces, interfaces, and membranes*. Addison-Wesley: Reading, 1994; Vol. 90.

(65) Balasubramanian, S. V.; Straubinger, R. M. Taxol-Lipid Interactions: Taxol-Dependent Effects on the Physical Properties of Model Membranes. *Biochemistry* **1994**, *33*, 8941-8947.

(66) Eichhorn, M. E.; Ischenko, I.; Luedemann, S.; Strieth, S.; Papyan, A.; Werner, A.; Bohnenkamp, H.; Guenzi, E.; Preissler, G.; Michaelis, U.; Jauch, K.-W.; Bruns, C. J.; Dellian, M. Vascular targeting by EndoTAG™-1 enhances therapeutic efficacy of conventional chemotherapy in lung and pancreatic cancer. *Int. J. Cancer* **2010**, *126*, 1235-1245.

(67) Eichhorn, M. E.; Luedemann, S.; Strieth, S.; Papyan, A.; Ruhstorfer, H.; Haas, H.; Michaelis, U.; Sauer, B.; Teifel, M.; Enders, G. H.; Brix, G.; Jauch, K. W.; Bruns, C. J.; Dellian, M. Cationic lipid complexed camptothecin (EndoTAG®-2) improves antitumoral efficacy by tumor vascular targeting. *Cancer Biology & Therapy* **2007**, *6*, 920-929.

(68) Li, Z.; Sun, L.; Zhang, Y.; Dove, A. P.; O'Reilly, R. K.; Chen, G. Shape Effect of Glyco-Nanoparticles on Macrophage Cellular Uptake and Immune Response. *ACS Macro Lett.* **2016**, *5*, 1059-1064.